



HAL
open science

Digital generation of single tone FM/PM test stimuli: a theoretical analysis

Kamilia Tahraoui, Florence Azaïs, Laurent Latorre, François Lefèvre,
Thibault Vayssade

► To cite this version:

Kamilia Tahraoui, Florence Azaïs, Laurent Latorre, François Lefèvre, Thibault Vayssade. Digital generation of single tone FM/PM test stimuli: a theoretical analysis. LATS 2024 - IEEE 25th Latin American Test Symposium, Apr 2024, Maceio, Brazil. pp.1-6, 10.1109/LATS62223.2024.10534627 . lirmm-04689333

HAL Id: lirmm-04689333

<https://hal-lirmm.ccsd.cnrs.fr/lirmm-04689333v1>

Submitted on 5 Sep 2024

HAL is a multi-disciplinary open access archive for the deposit and dissemination of scientific research documents, whether they are published or not. The documents may come from teaching and research institutions in France or abroad, or from public or private research centers.

L'archive ouverte pluridisciplinaire **HAL**, est destinée au dépôt et à la diffusion de documents scientifiques de niveau recherche, publiés ou non, émanant des établissements d'enseignement et de recherche français ou étrangers, des laboratoires publics ou privés.

Digital generation of single-tone FM/PM test stimuli: a theoretical analysis

K. Tahraoui ⁽¹⁾, F. Azais ⁽¹⁾, L. Latorre ⁽¹⁾, F. Lefevre ⁽²⁾, T. Vayssade ⁽¹⁾

⁽¹⁾ LIRMM, Univ. Montpellier, CNRS, 161 rue Ada, Montpellier, France

⁽²⁾ NXP Semiconductors, 2 Espl. Anton Phillips, 14000 Caen, France

Abstract— This paper presents a theoretical analysis for the generation of single-tone FM/PM test stimuli using a standard digital Automated Test Equipment (ATE). The technique relies on the generation of a modulated digital signal and the isolation of one of its harmonic replicas. The analysis conducted in this paper permits the appropriate setting of the digital signal parameters as well as the selection of favorable ATE sampling conditions.

Keywords—test signal generation; digital ATE; sampling theory; frequency/phase modulation

I. INTRODUCTION

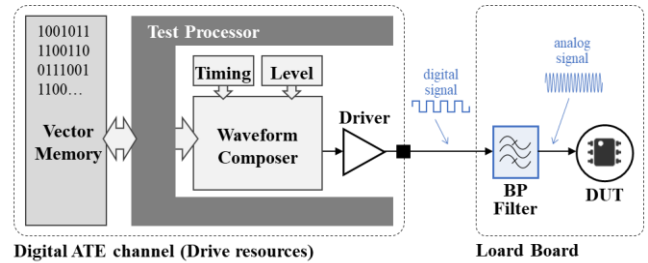
Wireless communications are ubiquitous in several applications ranging from consumer appliances to WSN (wireless sensor network) and IoT (Internet of Things). The physical layer of these communications is driven by Systems on Chip (SoCs) embedding an RF front-end that performs signal shaping, mostly based on narrow-band modulation schemes such as FSK, PSK or their numerous improved variants. Standards including Wi-Fi, Bluetooth, or Zigbee are good examples. As costs are squeezed at the application level, SoC manufacturer are seeking competitiveness by reducing their production expenses. In particular, the test of RF front-end represents a bottleneck in the batch production chain, requiring dedicated expensive high-end instrumentation and therefore limiting the ability to deploy parallel (multi-site) testing.

An interesting approach to reduce the testing costs is to develop digital solutions, as preconized by the ITRS. A number of works can be found in the literature, including the use of BIST within the circuit [1], modification of the ATE architecture [2], or dedicated analysis of analog/RF test responses using standard digital test resources [3-5]. The literature is less prolix regarding generation of analog/RF test stimuli using digital resources and mainly targets generation of sine-wave or multi-tone signals [6,7]. In this work, we target the generation of modulated signals following the approach introduced in [8] for the generation of OQPSK test stimuli. Our objective in this paper is to have a theoretical understanding using a simple modulation scheme, i.e. single-tone FM/PM.

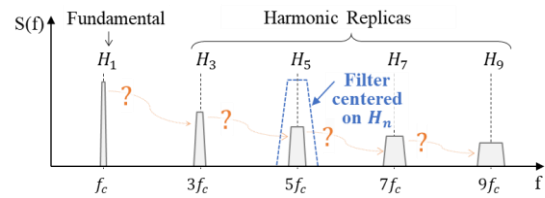
II. STRATEGY FOR DIGITAL TEST STIMULUS GENERATION

Our strategy to reduce analog/RF testing costs is to propose new solutions that can be applied with standard digital tester channels instead of analog/RF instruments. The targeted solution is illustrated in Figure 1. The basic principle is to generate a modulated digital signal using the standard resources of a digital ATE channel. A characteristic of a modulated digital signal is that, in addition to the baseband spectrum, it also exhibits harmonic replicas located at odd multiples of the signal frequency. The idea is to filter one of these harmonic replicas

to obtain the modulated analog signal. The filter can be placed on the load board, which provides the interface between the ATE and the device under test (DUT), and is the only analog resource required.



(a) Hardware resources



(b) Harmonic filtering of the digital signal

Fig. 1: Targeted solution for digital generation of the test stimulus

Note that a possibility is to directly encode the desired modulation in the digital signal and to filter the baseband spectrum. However, the frequency of the generated signal is obviously limited by the maximum value of the ATE operating frequency. By exploiting harmonic replicas, we can bypass this limitation and generate high-frequency test stimuli. However; it is necessary to understand how the amplitude and the spectral content of the harmonic replicas relate to the baseband spectrum in order to encode appropriate information in the modulated digital signal. The impact of ATE sampling conditions on the quality of the generated signal have also to be taken into account. Both aspects are addressed in this paper.

III. THEORETICAL DEVELOPEMENTS

A. Background on single-tone FM/PM modulation

A single-tone frequency-modulated (FM) or phase-modulated (PM) signal corresponds to a sinusoidal carrier signal whose phase or frequency varies according to the information of a sinusoidal message signal. In the general form, it can be expressed with:

$$y(t) = A \cos(\Phi(t)) = A \cos(\omega_c t + \beta \sin(\omega_m t)) \quad (1)$$

where $\Phi(t)$ is the instantaneous phase of the modulated signal, A is the amplitude of the carrier signal, ω_c and ω_m are the angular frequency of the carrier and message signals, and β is

the modulation index. This expression is valid for both FM and PM signals, only the definition of the modulation index differs: $\beta_{FM} = k_f A_m / \omega_m$ and $\beta_{PM} = k_p A_m$, where A_m is the message amplitude, k_f (in radians/volt-sec) and k_p (in radians/volt) being the deviation sensitivity.

By developing the cosine term of Eq.1 and using the Jacobi expansion, another expression can be obtained, involving Bessel coefficients:

$$y(t) = A \sum_{n=-\infty}^{\infty} J_n(\beta) \cos(2\pi(f_c + n f_m)t) \quad (2)$$

This expression reveals that the spectrum of a frequency or phase-modulated signal comprises a central component at the carrier frequency f_c and a series of sidebands located on both sides of the carrier frequency at $f_c \pm n f_m$, whose magnitudes are determined by the Bessel coefficients $J_n(\beta)$.

The spectrum can significantly differ depending on the modulation index, but globally the number of sidebands that hold significant power increases (i.e. the required bandwidth to transmit the signal) as the modulation index increases. The empirical Carson's rule defines the effective transmission band B_T ($\approx 98\%$ or more of transmitted power) with:

$$B_T = 2(\beta + 1)f_m \quad (3)$$

B. Stimulus generation from baseband digital carrier

As introduced in section II, the principle of our strategy is to generate a baseband modulated digital signal and to exploit one of its harmonic replicas to get a signal at higher frequency. Conceptually, a modulated digital signal can be obtained by applying a zero-crossing operation on a modulated analog signal. Indeed, the zero-crossing operation performs 1-bit quantization of the analog signal, i.e. it converts the analog signal into a binary signal with a high logic level at every time the analog signal is higher than zero and a low logic level at every time it is below. Note that the amplitude of the resulting digital signal can be freely adjusted by choosing the voltage values associated with low and high levels. In the following, unless specified, we will consider a symmetrical signal of amplitude A (i.e. high level at $+A$ and low level at $-A$). In this section, we analyze the effects of the 1-bit quantization process, in particular on the resulting harmonic replicas.

Let us first consider zero-crossing operation applied on an ideal sine-wave carrier of amplitude A_c and frequency f_c . The resulting signal is an ideal square-wave signal at the same frequency f_c . Using Fourier series expansion, this signal can be expressed as an infinite sum of sinusoids:

$$x_c(t) = \frac{4}{\pi} \left(A \cos(\omega_c t) + \frac{A}{3} \cos(3\omega_c t) + \frac{A}{5} \cos(5\omega_c t) + \dots \right) \quad (4)$$

where A is the square-wave amplitude and $\omega_c = 2\pi f_c$.

From this well-known expression, it can be seen that the zero-crossing operation creates harmonic tones located at odd multiples of the baseband carrier frequency, whose amplitude is reduced by the harmonic order.

In the same way, we can express a modulated digital signal as an infinite sum of modulated analog signals:

$$y(t) = \frac{4}{\pi} \left(A \cos(\Phi(t)) + \frac{A}{3} \cos(3\Phi(t)) + \frac{A}{5} \cos(5\Phi(t)) + \dots \right) \quad (5)$$

Referring to Eq.1, in case of FM/PM modulation, the instantaneous phase $\Phi(t)$ is given by:

$$\Phi(t) = \omega_c t + \beta \sin(\omega_m t) \quad (6)$$

Inserting this expression in Eq.5, the modulated digital signal is given by:

$$y(t) = \frac{4}{\pi} \left(A \cos(\omega_c t + \beta \sin(\omega_m t)) + \frac{A}{3} \cos(3\omega_c t + 3\beta \sin(\omega_m t)) + \frac{A}{5} \cos(5\omega_c t + 5\beta \sin(\omega_m t)) + \dots \right) \quad (7)$$

which can be re-expressed as:

$$y(t) = \frac{4}{\pi} \sum_i \frac{A}{i} \cos(2\pi i f_c t + i\beta \sin(2\pi f_m t)) \text{ for } i = 1, 3, 5, \dots \quad (8)$$

This expression clearly reveals that a modulated digital signal is a sum of modulated analog signals located at odd multiples of the baseband signal, with a modification of both the amplitude and the modulation index for each individual modulated analog signal.

As an illustration, Figure 2 shows the spectrum obtained from an FFT applied on a zero-crossed FM analog signal with $f_c = 100\text{MHz}$, $f_m = 3\text{MHz}$ and $\beta = 0.1$, the amplitude of the digital signal being set to $A_c = \pi/4$. As expected, the spectrum exhibits several replicas centered on odd multiples of the carrier frequency, each replica presenting sidebands located at $i f_c \pm n f_m$. The baseband spectrum has exactly the same characteristics than the spectrum of the original modulated analog signal, while the replicas are a transformed version of the baseband spectrum, with modification both in terms of spectral content and amplitude. For each replica, the harmonic order comes as multiplier for the modulation index and as a divider for the amplitude of the spectral components.

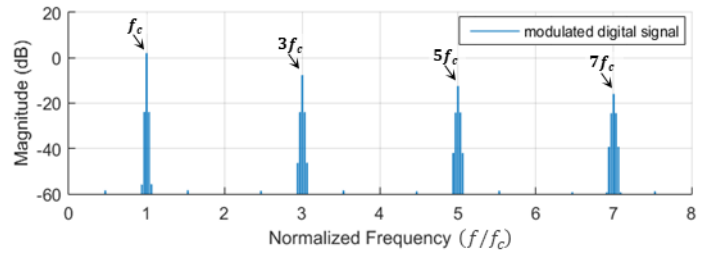


Fig.2: Spectrum of the modulated digital signal obtained from zero-crossing of a modulated analog signal

Going back to Eq.8 and introducing the Jacobi expansion, another expression of the modulated digital signal can be determined:

$$y(t) = \frac{4}{\pi} \sum_i \frac{A_c}{i} \left[\sum_{n=-\infty}^{\infty} J_n(i\beta) \cos(2\pi(i f_c + n f_m) t) \right] \text{ for } i = 1, 3, 5, \dots \quad (9)$$

Figure 3 shows the comparison between the spectrum obtained from an FFT applied on the modulated digital signal and the one derived from the values of the Bessel coefficients involved in Eq.9, with a zoom around the carrier frequency and the first two replicas. A perfect match can be observed for both the central frequency and the sidebands amplitude.

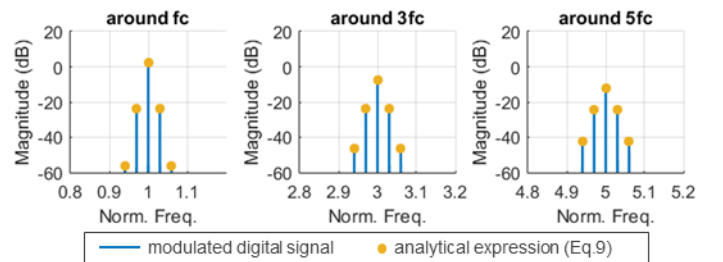


Fig.3: Zoom around the carrier frequency and the first two odd replicas

Eq.9 is a key element of the proposed strategy because it establishes the link between the spectral content and the amplitude of a given replica and the parameters used for the modulation of the baseband digital signal. It therefore permits to choose appropriate settings of the baseband signal to reach desired characteristics around a given replica. Practically, to obtain a modulated signal with carrier frequency $f_{c_{target}}$, carrier amplitude $A_{c_{target}}$ and modulation index β_{target} , the baseband digital signal should be generated with $f_c = f_{c_{target}}/i$, $A_c = \pi i A_{c_{target}}/4$ and $\beta = \beta_{target}/i$, where i is the order of the selected harmonic replica.

C. Stimulus generation using sampled-time digital system

So far, we have been dealing with continuous-time signals whose variations are also defined in the continuous-time domain, even in the case of the modulated digital signal. In our specific context, the stimulus will be generated by a digital Automatic Test Equipment (ATE), which is a discrete-time system. It means that the generated signal will be a continuous-time signal whose transitions are controlled by synchronous discrete events. Indeed, as shown in Figure 1, the general ATE architecture regarding digital signal generation involves a memory, a test processor, a waveform composer associated with timing and level formatters and a driver. The electrical signal delivered by the driver depends on both the digital data stored in the vector memory and the programmed timing and level information. Timing information includes the definition of the tester period (T_{cycle}), which gives the duration of one bit contained in the vector memory. Level information includes the definition of the voltage values used to drive a high level (V_{IH}) and a low level (V_{IL}). The test processor reads the content of the vector memory and formats it according to the programmed timing and level information. The resulting signal is then a binary signal with an amplitude $A = (V_{IH} - V_{IL})/2$, whose transitions occur on a time grid determined by the operating ATE frequency $f_{ATE} = 1/T_{cycle}$. In the following, we assume a symmetrical signal with $V_{IL} = -V_{IH}$.

Conceptually as depicted in Figure 4, the continuous-time signal generated by a digital ATE channel can be derived from a continuous-time analog signal modified by three successive operations, i.e. zero-crossing (ZC), sampling (S) and Zero-Order Hold (ZOH). In this section, we analyze the effects of the sampling and zero-order hold operations, when applied on a continuous-time digital signal.

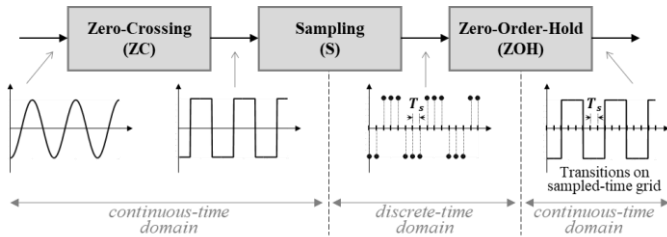


Fig.4: Continuous-time signal generated by a digital ATE channel

Sampling is the process of converting a continuous-time signal into a discrete sequence of samples. Mathematically, the sampled signal can be expressed as the multiplication of the analog signal $x(t)$ by a Dirac comb $\text{III}_{T_s}(t)$:

$$x_s(t) = x(t) * \text{III}_{T_s}(t) = x(t) * \sum_{k=-\infty}^{+\infty} \delta(t - kT_s) \quad (10)$$

Taking the Fourier transform, the expression in the frequency domain is given by:

$$\begin{aligned} X_s(f) &= X(f) \otimes \frac{1}{T_s} \text{III}_{f_s}(f) = X(f) * \frac{1}{T_s} \sum_{k=-\infty}^{+\infty} \delta(f - kf_s) \\ &= \frac{1}{T_s} \sum_{k=-\infty}^{+\infty} X(f - kf_s) \end{aligned} \quad (11)$$

As indicated by Eq.11, sampling induces a periodization of the spectrum, with copies of the original spectrum (called images) shifted by multiples of the sampling frequency and summed. This expression is the basis of the Nyquist theorem that states that a band-limited signal can be fully represented if sampled at a frequency f_s which is greater than twice the maximum frequency component f_M in the signal: $f_s > 2 * f_M$. Indeed, when this criterion is satisfied, there is no overlap between the baseband spectrum and the images created by the sampling process. An extension of the Nyquist theorem concerns narrowband signals, i.e. signals that have a limited bandwidth around a given frequency and that do not extent to DC. In this case, it is possible to sample the signal below the Nyquist rate while still obtaining a perfect signal representation in the Nyquist band, upon specific conditions on the sampling frequency. Such process is called undersampling, harmonic sampling or bandpass sampling.

Zero-order hold is the process converting a sampled signal to the continuous-time domain by maintaining each sample until the next one. Mathematically, this is expressed by a convolution between the sampled signal $x_s(t)$ and a rectangular function $\Pi_{T_s}(t - \frac{T_s}{2})$, where T_s is the sampling period:

$$\begin{aligned} x_{S-ZOH}(t) &= x_s(t) \otimes \Pi_{T_s}(t - \frac{T_s}{2}) \\ &= [x(t) * \text{III}_{T_s}(t)] \otimes \Pi_{T_s}(t - \frac{T_s}{2}) \end{aligned} \quad (12)$$

Taking the Fourier transform, the expression in the frequency domain is given by:

$$\begin{aligned} X_{S-ZOH}(f) &= \left[\frac{1}{T_s} \sum_{k=-\infty}^{+\infty} X(f - kf_s) \right] * T_s * \text{sinc}(\pi T_s f) * e^{-i\pi T_s f} \\ &= \text{sinc}(\pi T_s f) * e^{-i\pi T_s f} \sum_{k=-\infty}^{+\infty} X(f - kf_s) \end{aligned} \quad (13)$$

The zero-order hold process therefore introduces a global shaping of the periodized spectrum by the sinc function.

In our context, the modulated digital signal obtained from zero-crossing has theoretically an infinite number of replicas, so an infinite bandwidth. However, each replica is a narrow-band signal. So depending on the value of the sampling frequency, some replicas will satisfy the Nyquist criterion while others will be undersampled. Therefore, it might exist specific conditions on the sampling frequency that permits to avoid spectral corruption of a given harmonic replica. It is our objective to identify such conditions. We also have to take into account the sinc shaping introduced by the conversion of the sampled signal to the continuous time domain.

Let us first investigate the effects of the sample-and-hold operations on a non-modulated digital signal, i.e. a simple square-wave signal. For the following analysis, the ratio between the sampling frequency and the signal one is defined as the Number of Samples Per Period $NSPP = f_s/f_c$. Figure 5 shows the spectrum of the sampled-and-held signal for an

arbitrary value of $NSPP = 6.3$. The expected harmonic tones at odd multiples of the signal frequency are present but they are mixed with other components of similar or even higher amplitude. The components of high amplitude actually correspond to high-frequency images of the harmonic tones located below the Nyquist frequency, while the other additional components correspond to low-frequency images of the harmonic tones located above the Nyquist frequency (harmonic tones of order superior or equal to 5 for this example). Because on this example the $NSPP$ is a non-integer value, these images do not necessarily fall at odd multiples of the signal frequency; they are actually located at multiples of $0.1 * f_c$. The global shaping of the spectrum by the sin_c function which has local zeros at every multiple of the sampling frequency is also clearly observed; all components close to these local zeros are cancelled. In the context of the proposed strategy, care must be taken to ensure that useful information does not fall close to these local zeros. In particular, the sampling frequency must not be (and preferably not close to) a sub-multiple or multiple of the targeted replica frequency.

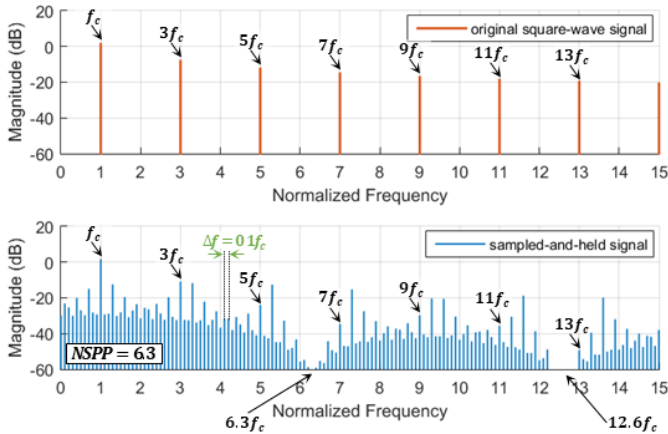


Fig.5: Spectrum comparison between original square-wave signal and sampled-and-held signal with $NSPP = 6.3$

Our objective is to establish an analytical expression of the sampled-and-held signal spectrum so that we can easily investigate the transformations brought on the original spectrum depending on the $NSPP$ value. Referring to the sampling theory, we can express the sampled-and-held signal as a square-wave signal multiplied by a Dirac comb $\text{III}_{T_s}(t)$ (sampling operation), which is convoluted with a rectangular function $\Pi_{T_s}(t - \frac{T_s}{2})$ (hold operation).

For the sake of simplicity, we consider a shifted and scaled version of the square-wave signal whose amplitude varies between 0 and 1 (the actual square-wave signal has an amplitude that varies between $+A$ and $-A$), which can be modeled by a convolution product between a rectangular function $\Pi_{T/2}(t)$ and a Dirac comb $\text{III}_T(t)$:

$$x_c(t) = \Pi_{T/2}(t) \otimes \text{III}_T(t) \quad (14)$$

where $T = 1/f_c$ is the period of the square-wave signal.

The sampled-and-held signal can therefore be expressed by:

$$\tilde{x}_c(t) = \left[\left(\Pi_{T/2}(t) \otimes \text{III}_T(t) \right) * \text{III}_{T_s}(t) \right] \otimes \Pi_{T_s} \left(t - \frac{T_s}{2} \right) \quad (15)$$

Using the Fourier transform, the signal in the frequency domain is:

$$\tilde{X}_c(f) = \left[\left(\frac{T}{2} * \text{sin}_c \left(\frac{\pi T f}{2} \right) * \frac{1}{T} \text{III}_{f_c}(f) \right) \otimes \frac{1}{T_s} \text{III}_{f_s}(f) \right] * T_s * \text{sin}_c(\pi T_s f) * e^{-i\pi T_s f} \quad (16)$$

Then:

$$\tilde{X}_c(f) = \left[\left(\frac{1}{2} \text{sin}_c \left(\frac{\pi T f}{2} \right) \sum_{k=-\infty}^{+\infty} \delta(f - k f_c) \right) \otimes \sum_{l=-\infty}^{+\infty} \delta(f - l f_s) \right] * \text{sin}_c(\pi T_s f) * e^{-i\pi T_s f} \quad (17)$$

After manipulation and simplification, it comes:

$$\tilde{X}_c(f) = \frac{1}{2} e^{-i\pi T_s f} \sum_{k=-\infty}^{+\infty} \sum_{l=-\infty}^{+\infty} \text{sin}_c \left(\pi \frac{k}{2} \right) * \text{sin}_c \left(\pi \left(k \frac{T_s}{T} + l \right) \right) * \delta(f - (k f_c + l f_s)) \quad (18)$$

By using the greatest common divisor between the signal frequency and the sampling frequency $\Delta f = \text{gcd}(f_c, f_s)$, we can re-express the term in the Dirac function:

$$k f_c + l f_s = (kx + ly) \Delta f \quad \text{with } x = f_c / \Delta f \text{ and } y = f_s / \Delta f \quad (19)$$

Introducing this form in Eq.18, the final expression of the sampled-and-held signal is:

$$\tilde{X}_c(f) = \frac{1}{2} e^{-i\pi T_s f} \sum_{k=-\infty}^{+\infty} \sum_{l=-\infty}^{+\infty} A_{k,l} \delta(f - (kx + ly) \Delta f) \quad \text{with } A_{k,l} = \text{sin}_c \left(\pi \frac{k}{2} \right) * \text{sin}_c \left(\pi \left(\frac{k}{NSPP} + l \right) \right) \quad (20)$$

This expression clearly establishes that the spectrum of the sampled-and-held square-wave signal exhibits frequency components located at multiples of Δf , whose amplitude depends on the $NSPP$ value.

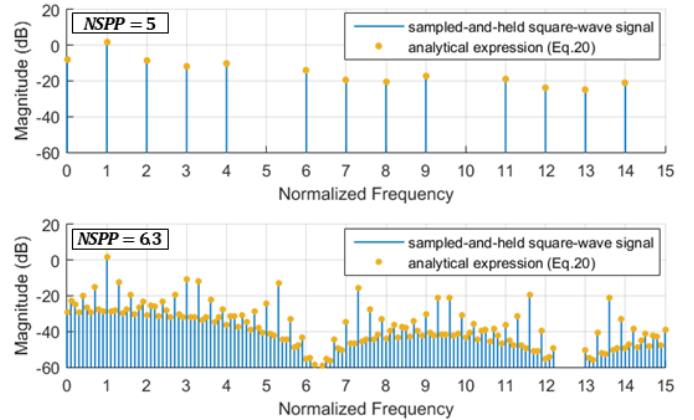


Fig.6: Comparison between the spectrum obtained from an FFT on the continuous-time digital signal obtained after sample and hold operations and the one derived from the analytical expression

Figure 6 shows the comparison between the spectrum computed with an FFT applied on the continuous-time digital signal obtained after sample and hold operations and the one computed with Eq.20 (a factor $2A$ has been applied on the amplitude to take into account a symmetrical square-wave signal with an amplitude that varies between $+A$ and $-A$), for an integer and a non-integer value of $NSPP$. In both cases, a perfect match can be observed both on the amplitude and the location of the spectral components. Note that in case of an integer $NSPP$ value, $\Delta f = \text{gcd}(f_c, f_s) = f_c$, which means that all the images of the harmonic tones fall at multiples of the baseband signal frequency f_c . The amplitude at a given multiple of the baseband signal frequency therefore corresponds to the

sum of the original tone plus the contribution of all the folded images. Note also that even harmonics appear in case of odd $NSPP$ value, due to folded components that fall at even multiples of the baseband signal frequency. In case of a rational $NSPP$ value, only a limited number of folded images fall at multiples of the baseband signal frequency and might bring only a negligible contribution compared to the original tone. This is specifically the case with the chosen $NSPP = 6.3$.

Finally, let us have a look at the effects of the sample-and-hold operations on a modulated digital signal, whose analytical expression has been established in the previous section (Eq.9). As in the case of a simple square-wave signal, we expect that the harmonic replicas that contain the modulation sidebands will be present in the spectrum, but mixed with additional components created by the sampling process. The shaping by the sin_c function will also apply, which means that the amplitude of the spectral components will be affected. In particular, assuming that there is no overlap between a given harmonic replica and images of other replicas, the expected amplitude of the central and sideband components is given by:

$$A_{i,n}^{expected} = A * \frac{4J_{|n|}(i\beta)}{\pi i} * \text{sin}_c\left(\frac{\pi i}{NSPP}\right) \quad \text{for } i = 1, 3, 5, \dots \quad (21)$$

where i is the order of the replica and n the order of the sideband components located at $if_c \pm nf_m$ ($n = 0$ for the central component located at if_c).

Figure 7 illustrates the spectrum of the sampled-and-held modulated digital signal for different $NSPP$ values; the expected amplitude if no overlap is also plotted (dot markers).

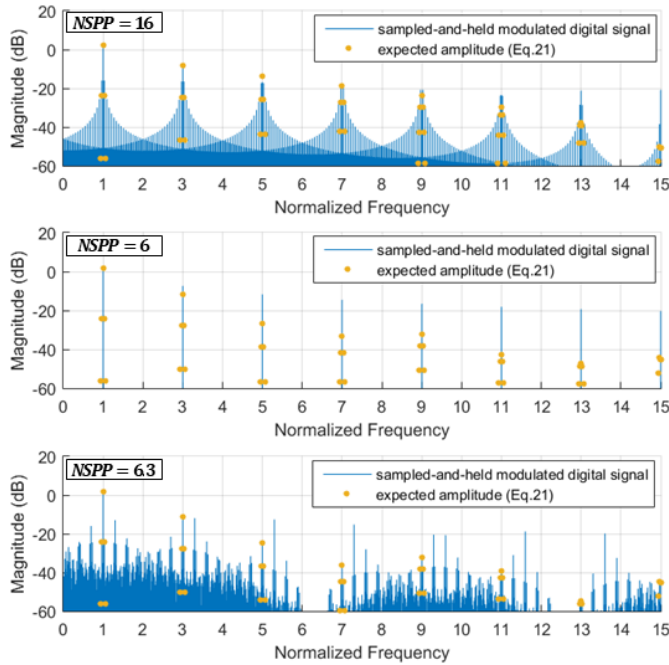


Fig.7: Spectrum comparison between original modulated digital signal and sampled-and-held signal for different $NSPP$ values

Several comments arise from this figure. First regarding the case of integer $NSPP$, harmonic replicas are observed at odd multiples of the carrier frequency when using $NSPP = 16$. However, the amplitude of the central and sideband components do not match with the expected one. Indeed in this case, images created by the sampling process are superimposed onto the existing replicas of the original signal. Since the modulation index changes with the replica order, the spectral

content of the original replicas is modified and no longer corresponds to the expected one. In case of $NSPP = 6$, only a single frequency component is observed at odd multiples of the carrier frequency. Indeed, when the $NSPP$ is not sufficiently high, the sampling process does not permit to capture the modulation effect (i.e. change in the instantaneous frequency) and simply converts the modulated square-wave into a non-modulated one. Obviously in the context of our strategy, both these situations should be avoided, which means that the sampling frequency must not be a multiple of the carrier frequency. Finally in case of $NSPP = 6.3$, the overall spectrum appears rather misted but the expected harmonic replicas are clearly visible and the amplitudes of the central and sidebands components are in good agreement with the expected ones. This example illustrates that despite all the modifications brought by the sample-and-hold process, it is possible to preserve the spectral content related to the modulation around the harmonic replicas, provided a pertinent choice of $NSPP$.

D. Conditions for non-destructive sampling

The main challenge is now to easily identify the values of the sampling frequency that allow non-destructive sampling for a given harmonic replica, i.e. no overlap between the targeted replica and images of other replicas with significant magnitude. The problem is highly complex, and all our attempts to derive a formal equation that expresses this condition have been unsuccessful so far. However, the analytical expression of the sampled-and-held digital carrier developed in the previous section (Eq.20) give us the opportunity of defining an estimator representative of the corruption around a given harmonic replica.

Basically, to avoid overlap between a given replica and images of other replicas, no image of the carrier harmonic tones should be present in neither the signal bandwidth $B_{T_i} = 2(i\beta + 1)f_m$, nor in its vicinity. The idea is therefore to compute, for the sampled-and-held digital carrier, the power contained in an enlarged bandwidth αB_{T_i} around each harmonic replica:

$$EBP_i = \sum_{j=-m}^m C_{i,m}^2 \quad (22)$$

where EBP stands for Enlarged Bandwidth Power, $C_{i,m}$ are all frequency components located at $if_c \pm m\Delta f$ comprised in the enlarged bandwidth $\left[if_c - \frac{\alpha B_{T_i}}{2}, if_c + \frac{\alpha B_{T_i}}{2}\right]$, and α is a factor higher than 1 that permits to choose to size of the enlarged bandwidth. For the following experiments, we arbitrarily choose $\alpha = 3$. In a practical situation, this factor should be chosen in accordance with the selectivity of the bandpass filter placed on the load board.

In ideal conditions, i.e. no image of the carrier harmonic tones present in this region, the power should be exactly the power of the original existing tone:

$$HCP_i^{expected} = H_i^2 = \left(\frac{4A}{\pi i} * \text{sin}_c\left(\frac{\pi i}{NSPP}\right)\right)^2 \quad (23)$$

where HCP stands for Harmonic Carrier Power

Based on these metrics, we define the corruption estimator associated with a given harmonic replica by:

$$Corr_Est_i = \frac{|EBP_i - HCP_i^{expected}|}{HCP_i^{expected}} \quad (24)$$

The numerator term is representative of the presence of images susceptible to interact with the considered replica. The denominator term acts as a penalty factor to account for the reduced amplitude as the replica order increases and the global \sin_c shaping induced by the hold process. In particular, the closer the replica i is from a local zero of the \sin_c function, the higher the penalty factor. Indeed, the proximity of a replica with a local zero entails a strong attenuation that might compromise baseband signal generation with sufficient amplitude.

This estimator permits to have a quantitative evaluation of the quality of the signal generated by the ATE around a given harmonic replica, for any potential sampling frequency. The closer this estimator is to zero, the better the quality of the generated signal.

IV. RESULTS

To illustrate the usefulness of this estimator, let us consider a digital modulated signal with $f_c = 100\text{MHz}$, $f_m = 3\text{MHz}$ and $\beta = 0.1$, the amplitude of the digital signal being set to $A_c = \pi/4$. The objective is to obtain, from this baseband digital signal, a modulated signal at 500MHz with a modulation index of 0.5, assuming a maximum ATE sampling frequency of 1.6GHz . Computation of the corruption estimator has been performed for the 5th harmonic replica varying the $NSPP$ value between 2 and 16 by step of 0.1. Results are summarized in Figure 8.

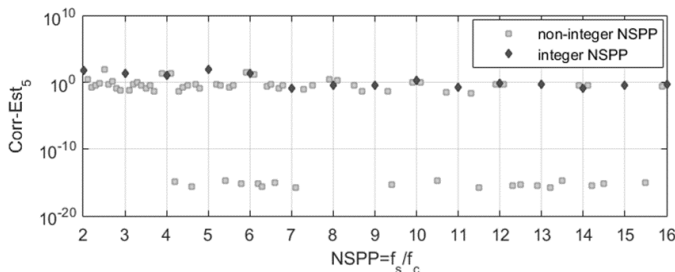


Fig.8: Corruption estimator vs. $NSPP$ for the 5th harmonic replica

Two main comments can be drawn from these results. First and as previously established, it is clear that the choice of an integer $NSPP$ is not a favorable condition. Second, it exists several $NSPP$ values that gives low corruption ($NSPP = 6.3$ used for illustration in previous figures is identified as a favorable condition), including low $NSPP$ values. This is of foremost importance since these values are the ones that impose the least constraints on the equipment capabilities. This estimator permits to identify them.

For this case study, the smallest $NSPP$ value that gives low corruption is $NSPP = 4.2$; this choice is therefore a priori a favorable condition to generate a good quality signal. This is confirmed by looking at the spectrum of the modulated digital signal obtained around the 5th harmonic (Figure 9). It can be observed that the central frequency and sideband components contained in the signal bandwidth are in good agreement with the expected values, indicating that the spectral content related to the desired modulation index is achieved. Moreover, the additional components contained in the signal bandwidth have an amplitude significantly lower than the one of the central frequency and sideband components. In the same way, all components contained in the enlarged bandwidth have an amplitude significantly lower than the one of the central frequency and sideband components. Note that it exists other

components with significant amplitude but they are outside the enlarged bandwidth; it is the role of the bandpass filter placed on the load board to eliminate these components.

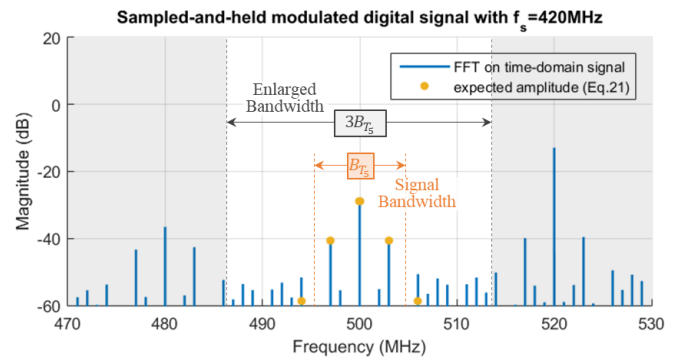


Fig.9: Spectrum of the sampled-and-held modulated digital signal with $NSPP = 4.2$ – Zoom around the 5th harmonic replica

More generally, this example shows that the proposed strategy permits to generate a modulated signal at a frequency even higher than the maximum ATE operating rate.

V. CONCLUSION

In this paper, we have explored an original approach for digital generation of FM/PM test stimuli. The basic principle is to use the standard resources of a digital ATE channel for the generation of a baseband modulated digital signal. The idea is then to filter one of the harmonic replicas produced by the digital signal to obtain a signal at higher frequency. Thanks to a theoretical analysis, the relation between the baseband spectrum and the harmonic replicas has been established, first in the continuous-time domain. The effects of sample-and-hold operations which are representative of the operating mode of a digital ATE have then been analyzed. An estimator has been defined that permits to easily identify the sampling conditions that minimize signal corruption. The proposed strategy has been evaluated in simulation and results have shown that the generation of a good quality modulated FM/PM signal can be achieved, even with limited sampling capabilities. Future work will target the hardware validation of this strategy and the extension to other modulation formats.

REFERENCES

- [1] C. H. Peng et al., "A novel RF self test for a combo SoC on digital ATE with multi-site applications," Proc. Int'l Test Conf. (ITC), pp. 1-8, 2014.
- [2] M. Ishida K. Ichiyama, "An ATE System for Testing RF Digital Communication Devices With QAM Signal Interfaces," IEEE Design & Test, vol. 33, no. 6, pp. 15-22, 2016.
- [3] N. Pous et al., J., "A Level-Crossing Approach for the Analysis of RF Modulated Signals using only Digital Test Resources", J. of Electronic Testing: Theory and App. (JETTA), vol. 27, no. 3, pp 289-303, 2011
- [4] S. David-Grignot et al., "Low-cost phase noise testing of complex RF ICs using standard digital ATE," Proc. Int'l Test Conf. (ITC), pp. 1-9, 2014.
- [5] T. Vayssade et al., "EVM measurement of RF ZigBee transceivers using standard digital ATE", Proc. Design, Automation & Test in Europe Conference (DATE), pp. 396-401, 2021.
- [6] H. Malloug et al., "Mostly digital design of sinusoidal signal generators for mixed-signal bist applications using harmonic cancellation," Proc. Int'l Mixed-Signal Testing Workshop (IMSTW), pp. 1-6, 2016.
- [7] S. David-Grignot et al., "Analytical study of on-chip generations of analog sine-wave based on combined digital signals," Proc. Int'l Mixed Signals Testing Workshop (IMSTW), pp. 1-5, 2017.
- [8] T. Vayssade et al., "Exploration of a digital-based solution for the generation of 2.4GHz OQPSK test stimuli," Proc. European Test Symp. (ETS), pp. 1-6, 2021.